

A microscopic calculation of asymmetric nuclear matter properties

D. Alonso and F. Sammarruca

Physics Department, University of Idaho, Moscow, ID 83844, U.S.A

(March 31, 2019)

A microscopic calculation of the equation of state for asymmetric nuclear matter is presented. We employ realistic nucleon-nucleon forces and operate within the Dirac-Brueckner-Hartree-Fock approach to nuclear matter. This work will merge naturally into the development of an effective interaction suitable for applications to asymmetric nuclei, which will be one of the focal point for nuclear physics in the future.

21.65.+f, 21.30.-x, 21.30.Fe

I. INTRODUCTION

Nuclear matter is an idealized uniform infinite system of protons and neutrons under their mutual strong forces and without electromagnetic interactions. Symmetric nuclear matter (that is, equal densities of protons and neutrons) has been studied extensively. The so-called conventional approach to nuclear matter goes back to earlier works by Brueckner and others [1-6] and is known as the BHF (Brueckner-Hartree-Fock) theory. During the 1980's, the Dirac-Brueckner-Hartree-Fock (DBHF) approach was developed [7-9]. The break-through came with the observation that the DBHF theory, unlike the conventional one, could describe successfully the saturation properties of nuclear matter, that is, saturation energy and density of the equation of state (EOS). The DBHF method adopts realistic nucleon-nucleon (NN) interactions and contains features of the relativistic theory. It characterizes the nuclear mean field by strong, competing scalar and vector fields that together account for the binding of nucleons as well as the large spin-orbit splitting seen in nuclear states. The DBHF framework is perhaps the most reliable, as well as feasible, microscopic method to describe effective interactions in the nuclear medium.

Asymmetric nuclear matter has been studied to a lesser degree. Systematic empirical investigations to determine the saturation properties of asymmetric matter have so far not been done. From the theoretical side, some older studies can be found in Refs. [10,11]. Interactions adjusted to fit properties of finite nuclei, such as those based on the non-relativistic Skyrme Hartree-Fock theory [12] or the relativistic mean field theory [13], have been used to extract phenomenological EOS. Generally, considerable model dependence is observed among predictions based on different EOS [14]. Variational calculations of asymmetric matter have also been reported [15].

The purpose of this paper is to present and describe microscopic calculations of the equation of state for asymmetric matter. We use realistic NN forces and operate within the DBHF framework. Recently, much interest has developed around the study of highly asymmetric nuclei (in particular, extremely neutron-rich nuclei, and halo nuclei). If approved for construction, the Rare Isotope Accelerator (RIA) will map the limits of nuclear existence

and allow the study of the unique nuclear systems which populate those boundaries. Thus, it is important and timely to develop microscopic effective interactions which can account for the asymmetry between proton and neutron densities.

In our self-consistent approach, a calculation of nuclear matter properties yields, at the same time, a convenient parametrization of the density dependence in the form of nucleon effective masses. This information can then facilitate the calculation of the scattering matrix at some positive energy, and finally of an effective interaction suitable, for example, for proton scattering on asymmetric nuclei. This interaction will be “isospin dependent”, in the sense of being different for the nn , pp , or np cases. Applications to scattering will be the next step in our pursuit.

Here, we will first describe our DBHF calculation of asymmetric matter (Section II). In Section III we will present and discuss results for the EOS at various levels of asymmetry. Conclusions and plans for future applications are presented in Section IV.

II. DESCRIPTION OF THE CALCULATION

Asymmetric nuclear matter can be characterized by the neutron density, ρ_n , and the proton density, ρ_p . It is also convenient to define the total density $\rho = \rho_n + \rho_p$ and the asymmetry (or neutron excess) parameter $\alpha = \frac{\rho_n - \rho_p}{\rho}$. Clearly, $\alpha=0$ corresponds to symmetric matter, and $\alpha=1$ to neutron matter.

In terms of α and the average Fermi momentum, related to the total density in the usual way,

$$\rho = \frac{2k_F^3}{3\pi^2}, \quad (1)$$

the neutron and proton Fermi momenta can be expressed as

$$k_F^n = k_F(1 + \alpha)^{1/3} \quad (2)$$

and

$$k_F^p = k_F(1 - \alpha)^{1/3}, \quad (3)$$

respectively.

We use the Thompson relativistic three-dimensional reduction of the Bethe-Salpeter equation. The Thompson equation is applied to nuclear matter in strict analogy to free-space scattering and reads, in the nuclear matter rest frame,

$$\begin{aligned} g_{ij}(\vec{q}', \vec{q}, \vec{P}, (\epsilon_{ij}^*)_0) &= v_{ij}^*(\vec{q}', \vec{q}) \\ &+ \int \frac{d^3K}{(2\pi)^3} v_{ij}^*(\vec{q}', \vec{K}) \frac{m_i^* m_j^*}{E_i^* E_j^*} \frac{Q_{ij}(\vec{K}, \vec{P})}{(\epsilon_{ij}^*)_0 - \epsilon_{ij}^*(\vec{P}, \vec{K})} g_{ij}(\vec{K}, \vec{q}, \vec{P}, (\epsilon_{ij}^*)_0) \end{aligned} \quad (4)$$

where $ij=nn$, pp , or np , and the asterix signifies that medium effects are applied to those quantities. In Eq. (4), \vec{q} , \vec{q}' , and \vec{K} are the initial, final, and intermediate relative momenta,

and $E_i^* = \sqrt{(m_i^*)^2 + K^2}$. The momenta of the two interacting particles in the nuclear matter rest frame have been expressed in terms of their relative momentum and the center-of-mass momentum, \vec{P} , through

$$\vec{P} = \frac{\vec{k}_1 + \vec{k}_2}{2} \quad (5)$$

$$\vec{K} = \frac{\vec{k}_1 - \vec{k}_2}{2} \quad (6)$$

The energy of the two-particle system is

$$\epsilon_{ij}^*(\vec{P}, \vec{K}) = e_i^*(\vec{P}, \vec{K}) + e_j^*(\vec{P}, \vec{K}) \quad (7)$$

and $(\epsilon_{ij}^*)_0$ is the starting energy. The single-particle energy e_i^* includes kinetic energy and potential energy, see below. The Pauli operator, Q , prevents scattering to occupied states. To eliminate the angular dependence from the kernel of Eq.(4), it is customary to replace the exact Pauli operator with its angle-average. Detailed expressions for the Pauli operator in the case of two different Fermi momenta are given in Appendix **A**. It is also customary to introduce an average center-of-mass momentum [5]. Definitions and details are also provided in Appendix **A**.

With the definitions

$$G_{ij} = \frac{m_i^*}{E_i^*(\vec{q}')} g_{ij} \frac{m_j^*}{E_j^*(\vec{q})} \quad (8)$$

and

$$V_{ij}^* = \frac{m_i^*}{E_i^*(\vec{q}')} v_{ij}^* \frac{m_j^*}{E_j^*(\vec{q})} \quad (9)$$

one can rewrite Eq.(4) as

$$\begin{aligned} G_{ij}(\vec{q}', \vec{q}, \vec{P}, (\epsilon_{ij}^*)_0) &= V_{ij}^*(\vec{q}', \vec{q}) \\ &+ \int \frac{d^3K}{(2\pi)^3} V_{ij}^*(\vec{q}', \vec{K}) \frac{Q_{ij}(\vec{K}, \vec{P})}{(\epsilon_{ij}^*)_0 - \epsilon_{ij}^*(\vec{P}, \vec{K})} G_{ij}(\vec{K}, \vec{q}, \vec{P}, (\epsilon_{ij}^*)_0) \end{aligned} \quad (10)$$

which is formally identical to the non-relativistic equation. We make use of the definitions Eqs.(8-9) throughout this paper, which is why all formulas involving the operator G appear identical to their non-relativistic equivalent.

The goal is to determine self-consistently the nuclear matter single-particle potential which, in our case, will be different for neutrons and protons. To facilitate the description of the numerical procedure, we will use a schematic notation for the neutron/proton potential (while the corresponding detailed expressions are reported in Appendix **B**). We write, for neutrons,

$$U_n = U_{np} + U_{nn} \quad (11)$$

and for protons

$$U_p = U_{pn} + U_{pp} \quad (12)$$

where each of the four pieces on the right-hand-side of Eqs.(11-12) depends on the appropriate G-matrix (nn , pp , or np) from Eq.(10). Clearly, the two equations above are coupled through the np component and so they must be solved simultaneously. Furthermore, the G-matrix equation and Eqs.(11-12) are coupled through the single-particle energy (which includes the single-particle potential). So we have three coupled equations to be solved self-consistently. As done in the symmetric case [9], we parametrize the single particle potential for protons and neutrons (Eqs.(11-12)) in terms of two constants, $U_{S,i}$ and $U_{V,i}$, (the scalar and vector potential) through

$$U_i(k_i) = \frac{m_i^*}{E_i^*} U_{S,i} + U_{V,i}. \quad (13)$$

For the purpose of facilitating the connection to the usual non-relativistic framework [5], it is customary to redefine $U_{S,i}$ and $U_{V,i}$ in terms of two other constants defined as

$$m_i^* = m_i + U_{S,i} \quad (14)$$

and

$$U_{0,i} = U_{S,i} + U_{V,i}. \quad (15)$$

The subscript “ i ” signifies that these parameters are different for protons and neutrons. Starting from some initial values of m_i^* and $U_{0,i}$, the G-matrix equation is solved and a first approximation for $U_i(k_i)$ is then obtained. This solution is again parametrized in terms of a new set of constants, and the procedure is repeated until convergence is reached. The effective masses for neutrons and protons, m_i^* , obtained through this procedure are shown in Figs. (1-2) as a function of the Fermi momentum at various levels of asymmetry.

Finally, the energy per neutron or proton in nuclear matter is calculated from

$$\bar{e}_i = \langle T_i \rangle + \langle U_i \rangle. \quad (16)$$

(See Appendix C for details.) The EOS, or energy per nucleon as a function of density, is then written as

$$\bar{e}(\rho_n, \rho_p) = \frac{\rho_n \bar{e}_n + \rho_p \bar{e}_p}{\rho} \quad (17)$$

or

$$\bar{e}(k_F, \alpha) = \frac{(1 + \alpha)\bar{e}_n + (1 - \alpha)\bar{e}_p}{2}. \quad (18)$$

III. PROPERTIES OF THE EQUATION OF STATE

The NN potential used in this work is the relativistic OBEP from Ref. [16] which uses the Thompson equation and the pseudo-vector coupling for the π and η mesons.

The EOS as obtained from our DBHF calculation is displayed in Fig. 3, as a function of k_F and for values of α between 0 and 1. The symmetric matter EOS saturates at $k_F \approx 1.4 fm^{-1}$ with a value of 16.7 MeV, in good agreement with the empirical values. For the compression modulus of saturated symmetric matter, defined as

$$\kappa = k_F^2 \frac{\partial^2 \bar{e}(k_F)}{\partial^2 k_F} \Big|_{k_F=k_F^{(0)}} \quad (19)$$

we find a value of 233 MeV. This is in excellent agreement with the recent empirical determination of 225 ± 15 MeV [17].

As the neutron density increases (the total density remaining constant), the EOS becomes increasingly repulsive and the minimum shifts towards lower densities. As the system moves towards neutron matter, the “energy well” gets more and more shallow, until, for α larger than about 0.8, the system is no longer bound.

We also show for comparison the EOS based on the BHF calculation, see Fig. 4. Also in this case we have performed a self-consistent calculation based on the same realistic force. However, no medium modifications are included in the potential to account for the proper Dirac structure of the nucleons in nuclear matter. As a consequence of that, saturation of symmetric matter is obtained at a much higher density, a well-known problem with the conventional approach.

In Fig. 5, we take a different look at the EOS. There, we plot the quantity $\bar{e}(k_F, \alpha) - \bar{e}(k_F, 0)$ versus α^2 . Clearly, the behaviour is linear, that is

$$\bar{e}(k_F, \alpha) - \bar{e}(k_F, 0) = e_s \alpha^2, \quad (20)$$

or parabolic versus α . This linear behaviour, shared with the non-relativistic predictions, see Fig. 6, is reminiscent of the asymmetry term in the familiar semi-empirical mass formula. By reading the slope of each line, we can then predict the nuclear symmetry energy, defined as

$$e_s = \frac{1}{2} \frac{\partial^2 \bar{e}(k_F, \alpha)}{\partial^2 \alpha} \Big|_{\alpha=0}. \quad (21)$$

This is shown in Fig. 7, where the solid curve is the prediction from the DBHF model and the dashed corresponds to the BHF calculation. The DBHF prediction at saturation density is about 30 MeV. Although in agreement at the lower densities, the two curves differ considerably at high density. Empirical constraints on the high-density behaviour of the nuclear symmetry energy would be very helpful. Energetic reactions induced by heavy neutron-rich nuclei have been proposed as a mean to obtain crucial information on the high-density behaviour of the nuclear symmetry energy and thus the EOS of dense neutron-rich matter [18].

IV. SUMMARY AND CONCLUSIONS

We have presented a microscopic calculation of the equation of state of nuclear matter when protons and neutrons have different Fermi momenta. The calculation is self-consistent and parameter-free, in the sense that no parameter of the NN force is adjusted in the medium.

As expected, the single-particle energy moves up to less attractive values to merge with the neutron matter equation of state when the proton density approaches zero. The dependence of the EOS on the neutron excess parameter is clearly linear as a function of α^2 . We make predictions for the nuclear symmetry energy and observe a large discrepancy between the relativistic and the non-relativistic predictions at high density.

A relatively simple way to relate the microscopic EOS directly to structural properties of finite nuclei is the use of a mass formula [14], where the “volume” term is directly related to the EOS. In that context, it has been pointed out [14] that, unlike proton densities, neutron densities are very sensitive to the EOS model. At the same time, precise data on neutron radii and neutron skins are not readily available to discriminate clearly among models. Even for a nucleus such as ^{208}Pb , for which a fairly large database exists, determinations of the neutron skins differ considerably from model to model [19]. We are presently in the process of probing our EOS through such calculations of neutron radii and neutron skins.

The relative simplicity of a homogeneous infinite system makes nuclear matter calculations a convenient starting point for the determination of an effective interaction suitable for finite nuclei. Together with the local density approximation, this approach has been used extensively and with success for proton-nucleus scattering. Our asymmetric matter G-matrix is now available for DWBA calculations of scattering on asymmetric nuclei.

Ultimately, the goal is to study nuclei with high levels of asymmetry, about which very little is known. Coherent effort from both the experimental and the theoretical side is necessary in order to combine reliable models of the density dependence of the effective nuclear force with reliable structure information. Hopefully, the RIA facility will be available in the near future to answer open questions and help us understand the physics of the weakly bound systems that are expected to exist at the limits of the nuclear chart.

ACKNOWLEDGMENTS

The authors acknowledge financial support from the U.S. Department of Energy under grant No. DE-FG03-00ER41148.

APPENDIX A: ELIMINATION OF THE ANGULAR DEPENDENCE

1. Angle-averaged Pauli operator

The definition of the Pauli operator is, for the case of two different Fermi momenta

$$Q = \begin{cases} 0 & \text{if } \begin{cases} k_\mu \leq k_F^n \\ \text{or} \\ k_\nu \leq k_F^p \end{cases} \\ 1 & \text{if } \begin{cases} k_\mu > k_F^n \\ \text{and} \\ k_\nu > k_F^p \end{cases} \end{cases} \quad (\mu \neq \nu = 1, 2) \quad (\text{A1})$$

In the angle-average approximation, one replaces the exact Q operator with its average over all angles for fixed P and K . That is, one defines

$$\tilde{Q} = \langle Q \rangle = \frac{\int Q(K, P, \theta) d\Omega}{\int d\Omega} = \frac{1}{2} \int_{\theta_1}^{\theta_2} Q(P, K, \theta) d\theta \quad (\text{A2})$$

The variables $\vec{P}, \vec{K}, \vec{k}_\mu$ are as defined previously, θ is the angle between \vec{P} and \vec{K} , and $Q \neq 0$ for $\theta_1 < \theta < \theta_2$.

Several cases can occur, depending on the values of K, P, k_F^p and k_F^n . Those are:

$$\tilde{Q} = \begin{cases} 0 & K^2 < \frac{1}{2}((k_F^n)^2 + (k_F^p)^2) - P^2 \\ 1 & (P - K)^2 > (k_F^n)^2 \\ \frac{1}{4PK} ((K + P)^2 - (k_F^n)^2) & (k_F^p)^2 < (P - K)^2 < (k_F^n)^2 \\ \frac{1}{2PK} (K^2 + P^2 - \frac{1}{2}((k_F^n)^2 + (k_F^p)^2)) & \text{otherwise} \end{cases} \quad (\text{A3})$$

2. Averaged center-of-mass momentum

To simplify the integration leading to the single-particle spectrum and the energy per particle (see Appendices **B** and **C**), we introduce the average center-of-mass momentum. This is defined as the root-mean-square value of P for two particles with the constraint that their relative momentum is K (case *a*), and, in addition, that one of the particles has momentum k_μ (case *b*).

a. K fixed

Definition of average c.m. momentum (K fixed):

$$P_{AV}^2 = \frac{\int_0^{k_F^n} d\vec{k}_1 \int_0^{k_F^p} d\vec{k}_2 P^2 \delta(K - \frac{1}{2} |\vec{k}_1 - \vec{k}_2|)}{\int_0^{k_F^n} d\vec{k}_1 \int_0^{k_F^p} d\vec{k}_2 \delta(K - \frac{1}{2} |\vec{k}_1 - \vec{k}_2|)} \quad (\text{A4})$$

To simplify the final expressions, we introduce the following notation

$$x = k_F^n + K \quad y = k_F^p - K \quad s = k_F^n - K \quad t = k_F^p + K \quad (\text{A5})$$

The final expression is then

$$P_{AV}^2 = \begin{cases} \frac{3}{5}(k_F^p)^2 + K^2 & K < k_F^p \\ \frac{8}{5}K(s^5 + y^5) + \frac{1}{12}(ty + sx)^3 + \frac{2}{3}(s^6 + y^6) - (ty^5 + sx^5) & \text{otherwise} \\ \frac{8}{3}K(s^3 + y^3) + \frac{1}{2}(ty + sx)^2 + (s^4 + y^4) - 2(ty^3 + sx^3) & (k_F^n + k_F^p) < 2K \\ 0 & \end{cases} \quad (\text{A6})$$

b. K and k_μ fixed

Definition of average c.m. momentum (K and k_μ fixed):

$$\tilde{P}_{AV}^2 = \frac{\int_{\Omega_\mu} d\Omega_\mu \int_0^{k_F^i} d\vec{k}_\nu P^2 \delta(K - \frac{1}{2} |\vec{k}_\mu - \vec{k}_\nu|)}{\int_{\Omega_\mu} d\Omega_\mu \int_0^{k_F^i} d\vec{k}_{2\nu} \delta(K - \frac{1}{2} |\vec{k}_\mu - \vec{k}_\nu|)} \quad (\text{A7})$$

$$\boxed{k_\mu < k_F^i}$$

$$\tilde{P}_{AV}^2 = \left\{ \begin{array}{ll} (k_\mu)^2 + K^2 & 2K < k_F^i - k_\mu \\ \frac{1}{4}(3(k_\mu)^2 + (k_F^i)^2 - 4Kk_\mu) & k_F^i - k_\mu < 2K < k_F^i + k_\mu \\ 0 & \text{otherwise} \end{array} \right\} \quad (\text{A8})$$

$$\boxed{k_\mu > k_F^i}$$

$$\tilde{P}_{AV}^2 = \left\{ \begin{array}{ll} \frac{1}{4}(3(k_\mu)^2 + (k_F^i)^2 - 4Kk_\mu) & k_\mu - k_F^i < 2K < k_F^i + k_\mu \\ 0 & \text{otherwise} \end{array} \right\} \quad (\text{A9})$$

where $\mu = 1, 2$ and $i=n$ or p .

APPENDIX B: NUCLEAR MATTER SINGLE-PARTICLE POTENTIAL

The single-particle potential in nuclear matter, U_i ($i=n$ or p), is defined in the usual way [20]

$$U_i(k_\mu) = \sum_{j < A} \langle \mu_i \nu_j | G^{ij} | \mu_i \nu_j - \nu_j \mu_i \rangle =$$

$$\sum_{j_1 < N} \langle \mu_i \nu_{j_1} | G^{in} | \mu_i \nu_{j_1} - \nu_{j_1} \mu_i \rangle + \sum_{j_2 < Z} \langle \mu_i \nu_{j_2} | G^{ip} | \mu_i \nu_{j_2} - \nu_{j_2} \mu_i \rangle \quad (\text{B1})$$

The explicit evaluation of this expression in partial-wave decomposition yields

$$\begin{aligned}
U_i(k_\mu) &= \frac{8\lambda}{\pi k_\mu} \sum_{L,\alpha} (2J+1) \mathcal{T}_{in}^T \left[\int_0^{\frac{k_F^n - k_\mu}{2}} K_0 dK_0 \int_{|k_\mu - K_0|}^{k_\mu + K_0} PdPG_{LL}^{\alpha, in}(P; K_0, K_0) \right. \\
&+ \left. \int_{\frac{k_F^n - k_\mu}{2}}^{\frac{k_F^n + k_\mu}{2}} K_0 dK_0 \int_{|k_\mu - K_0|}^{\sqrt{\frac{k_\mu^2 + (k_F^n)^2}{2} - K_0^2}} PdPG_{LL}^{\alpha, in}(P; K_0, K_0) \right] + \begin{pmatrix} n \longleftrightarrow p \\ k_F^n \longleftrightarrow k_F^p \end{pmatrix} \quad (B2)
\end{aligned}$$

(α stands for the quantum numbers J, S and T).

Using the averaged-momentum approximation (see Appendix A),

$$G_{LL}^{\alpha, ij}(P; K_0, K_0) \approx G_{LL}^{\alpha, ij}(\tilde{P}_{AV}; K_0, K_0), \quad (B3)$$

allows to simplify the integral over P, with the final result being

$$\begin{aligned}
U_i(k_\mu) &= \frac{8\lambda}{\pi k_\mu} \sum_{L,\alpha} (2J+1) \mathcal{T}_{in}^T \left[\int_0^{\frac{k_F^n - k_\mu}{2}} K_0 dK_0 G_{LL}^{\alpha, in}(\tilde{P}_{AV}; K_0, K_0) \int_{|k_\mu - K_0|}^{k_\mu + K_0} PdP \right. \\
&+ \left. \int_{\frac{k_F^n - k_\mu}{2}}^{\frac{k_F^n + k_\mu}{2}} K_0 dK_0 G_{LL}^{\alpha, in}(\tilde{P}_{AV}; K_0, K_0) \int_{|k_\mu - K_0|}^{\sqrt{\frac{k_\mu^2 + (k_F^n)^2}{2} - K_0^2}} PdP \right] + \begin{pmatrix} n \longleftrightarrow p \\ k_F^n \longleftrightarrow k_F^p \end{pmatrix} \\
&= \frac{16\lambda}{\pi} \sum_{L,\alpha} (2J+1) \mathcal{T}_{in}^T \left[\int_0^{\frac{k_F^n - k_\mu}{2}} K_0^2 dK_0 G_{LL}^{\alpha, in}(\tilde{P}_{AV}; K_0, K_0) \right. \\
&+ \left. \frac{1}{2k_\mu} \int_{\frac{k_F^n - k_\mu}{2}}^{\frac{k_F^n + k_\mu}{2}} K_0 dK_0 \left[\frac{(k_F^n)^2 - k_\mu^2}{4} - K_0(K_0 - k_\mu) \right] G_{LL}^{\alpha, in}(\tilde{P}_{AV}; K_0, K_0) \right] + \begin{pmatrix} n \longleftrightarrow p \\ k_F^n \longleftrightarrow k_F^p \end{pmatrix} \quad (B4)
\end{aligned}$$

The coefficients \mathcal{T}_{ij}^T contain the isospin dependence and are equal to

$$\begin{aligned}
\mathcal{T}_{np}^{T=0,1} &= \mathcal{T}_{pn}^{T=0,1} = \frac{1}{2}; & \mathcal{T}_{nn}^0 &= \mathcal{T}_{pp}^0 = 0; \\
\mathcal{T}_{nn}^1 &= \mathcal{T}_{pp}^1 = 1
\end{aligned}$$

APPENDIX C: ENERGY PER NUCLEON IN NUCLEAR MATTER

The energy per neutron/proton is:

$$\bar{e}_n = \langle T_n \rangle + \frac{1}{2N} \sum_{j < A} \sum_{i < N} \langle \mu_i \nu_j | G_{ij} | \mu_i \nu_j - \nu_j \mu_i \rangle \quad (C1)$$

$$\bar{e}_p = \langle T_p \rangle + \frac{1}{2Z} \sum_{j < A} \sum_{i < Z} \langle \mu_i \nu_j | G_{ij} | \mu_i \nu_j - \nu_j \mu_i \rangle \quad (C2)$$

which, in view of Eq.(B1), can be written as

$$\bar{e}_n = \langle T_n \rangle + \frac{1}{2N} \sum_{i < N} U_i(k_\mu) \quad (C3)$$

$$\bar{e}_p = \langle T_p \rangle + \frac{1}{2Z} \sum_{i < Z} U_i(k_\mu) \quad (C4)$$

By applying again the partial-wave decomposition and the average momentum approximation

$$G_{LL}^{\alpha,ij}(P; K_0, K_0) \approx G_{LL}^{\alpha,ij}(P_{AV}; K_0, K_0) \quad (C5)$$

the energy per neutron/proton is finally

$$\begin{aligned} \bar{e}_i = \langle T_i \rangle + \frac{6\lambda}{\pi(k_F^i)^3} \sum_{L,\alpha} (2J+1) & \left[\frac{4}{3} (k_F^p)^3 \mathcal{T}_{pn}^T \int_0^{\frac{k_F^n - k_F^p}{2}} K_0^2 dK_0 G_{LL}^{\alpha(np)}(P_{AV}; K_0, K_0) + \right. \\ & 2\mathcal{T}_{pn}^T \int_{\frac{k_F^n - k_F^p}{2}}^{\frac{k_F^n + k_F^p}{2}} K_0^2 dK_0 \left[\frac{(k_F^n)^3 + (k_F^p)^3}{3} - \frac{((k_F^n)^2 - (k_F^p)^2)^2}{16K_0} + \frac{K_0^3}{3} - \frac{K_0}{2} ((k_F^n)^2 + (k_F^p)^2) \right] \\ & \left. G_{LL}^{\alpha(np)}(P_{AV}; K_0, K_0) + \frac{2}{3} (k_F^i)^3 \mathcal{T}_{ii}^T \int_0^{k_F^i} K_0^2 dK_0 \left[2 - 3\frac{K_0}{k_F^i} + \left(\frac{K_0}{k_F^i}\right)^3 \right] G_{LL}^{\alpha(ii)}(P_{AV}; K_0, K_0) \right] \end{aligned} \quad (C6)$$

where, again, $i = n$ or p .

- [1] K.A. Brueckner, C.A. Levinson, and H.M. Mahmoud, Phys. Rev. **95**, 217 (1954).
- [2] H.A. Bethe, Phys. Rev. **103**, 1353 (1956).
- [3] J. Goldstone, Proc. R. Soc. London, Ser.A **239**,267 (1957).
- [4] H.A. Bethe, Annu. Rev. Nucl. Sci. **21**, 93 (1971).
- [5] M.I. Haftel and F. Tabakin, Nucl. Phys. **A158**, 1 (1970).
- [6] D.W.L. Sprung, Adv. Nucl. Phys. **5**, 225 (1972).
- [7] M.R. Anastasio, L.S. Celenza, W.S. Pong, and C.M. Shakin, Phys. Rep. **100**, 327 (1983).
- [8] C.J. Horowitz and B.D. Serot, Nucl. Phys. **A464**, 613 (1987).
- [9] R. Brockmann and R. Machleidt, Phys. Lett. **149B**, 283 (1984); Phys. Rev. C **42**, 1965 (1990).
- [10] K.A. Brueckner and S.A. Coon, Phys. Rev. **168**, 1184 (1968).
- [11] P.J. Siemens, Nucl. Phys. **A141**, 225 (1970).
- [12] M. Beiner, H. Flocard, Nguyen Van Giai, and P. Quentin, Nucl. Phys. **A238**, 29 (1975).
- [13] Y. Sugahara and H. Toki, Nucl. Phys. **A579**, 557 (1994).

- [14] K. Oyamatsu, I. Tanihata, Y. Sugahara, K. Sumiyoshi, and H. Toki, Nucl. Phys. **A634**, 3 (1998).
- [15] I.E. Lagaris and V.R. Pandharipande, Nucl. Phys. **A369**, 470 (1981).
- [16] R. Machleidt, Adv. Nucl. Phys. **19**, 189 (1989).
- [17] P. Danielowicz, preprint nucl-th/0203002.
- [18] Bao-An Li, Bulletin of the American Physical Society, Vol. 47, No. 6, p.96.
- [19] S. Karataglidis, K. Amos, B.A. Brown, and P.K. Deb, Phys. Rev. C **65**, 044306 (2002).
- [20] H. Bethe, B.H. Brandow, and A.G. Petschek, Phys. Rev. **129**, 225 (1963).

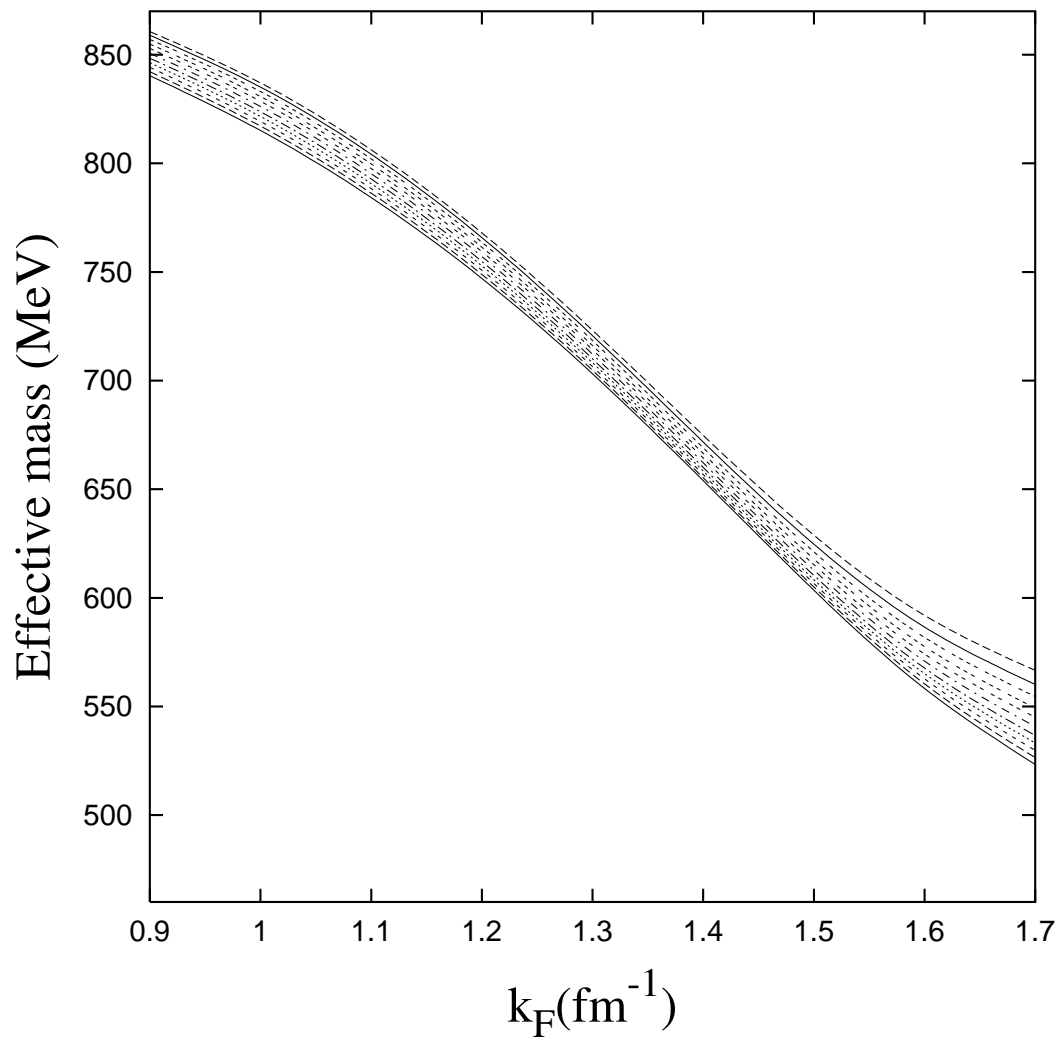


FIG. 1. Neutron effective masses as a function of the Fermi momentum and for increasing values of α between 0 and 1. The upper curve corresponds to $\alpha = 1$.

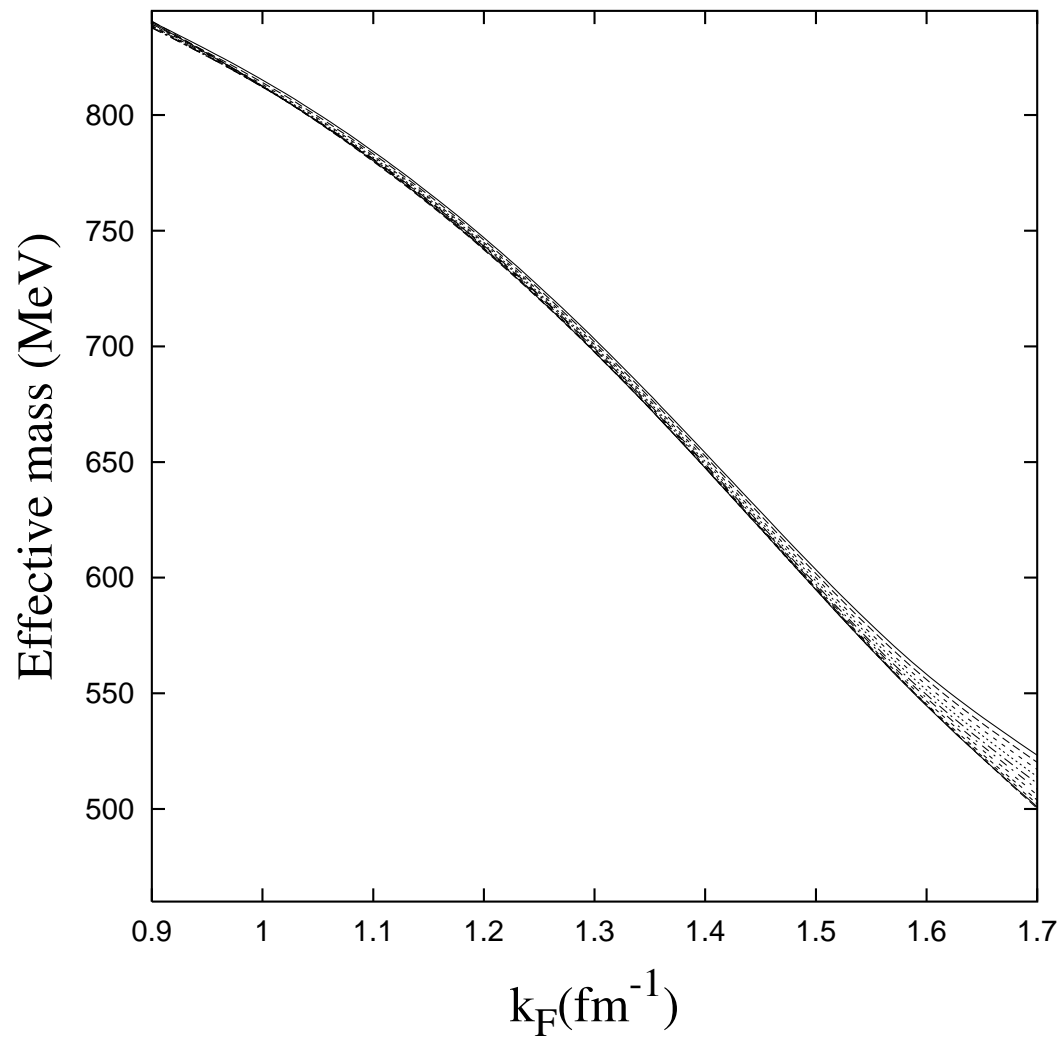


FIG. 2. As in Fig. 1, for protons. The upper curve corresponds to $\alpha = 0$.

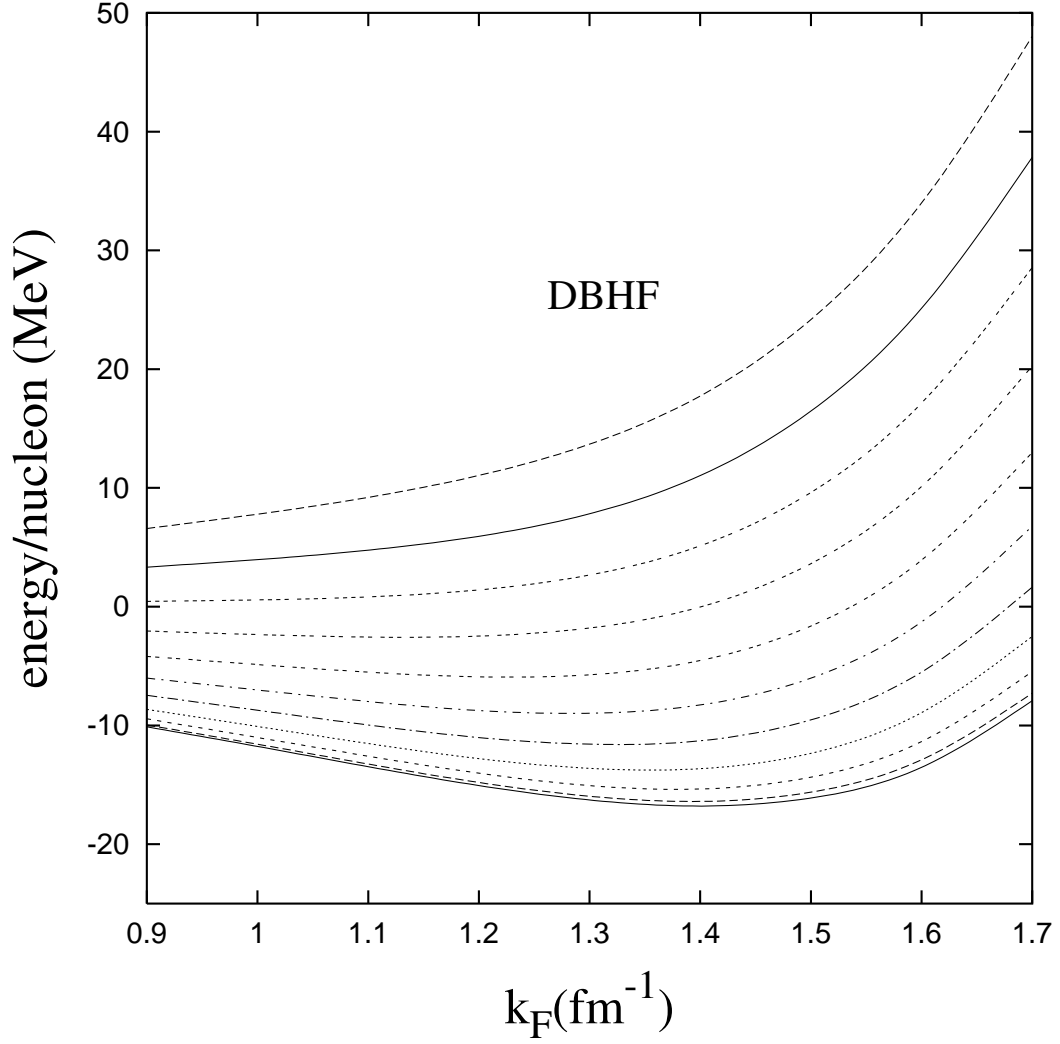


FIG. 3. Energy per nucleon as a function of the Fermi momentum at different values of the asymmetry parameter (in steps of 0.1) from symmetric matter (lowest curve) to neutron matter (highest curve). The predictions are obtained from DBHF calculation.

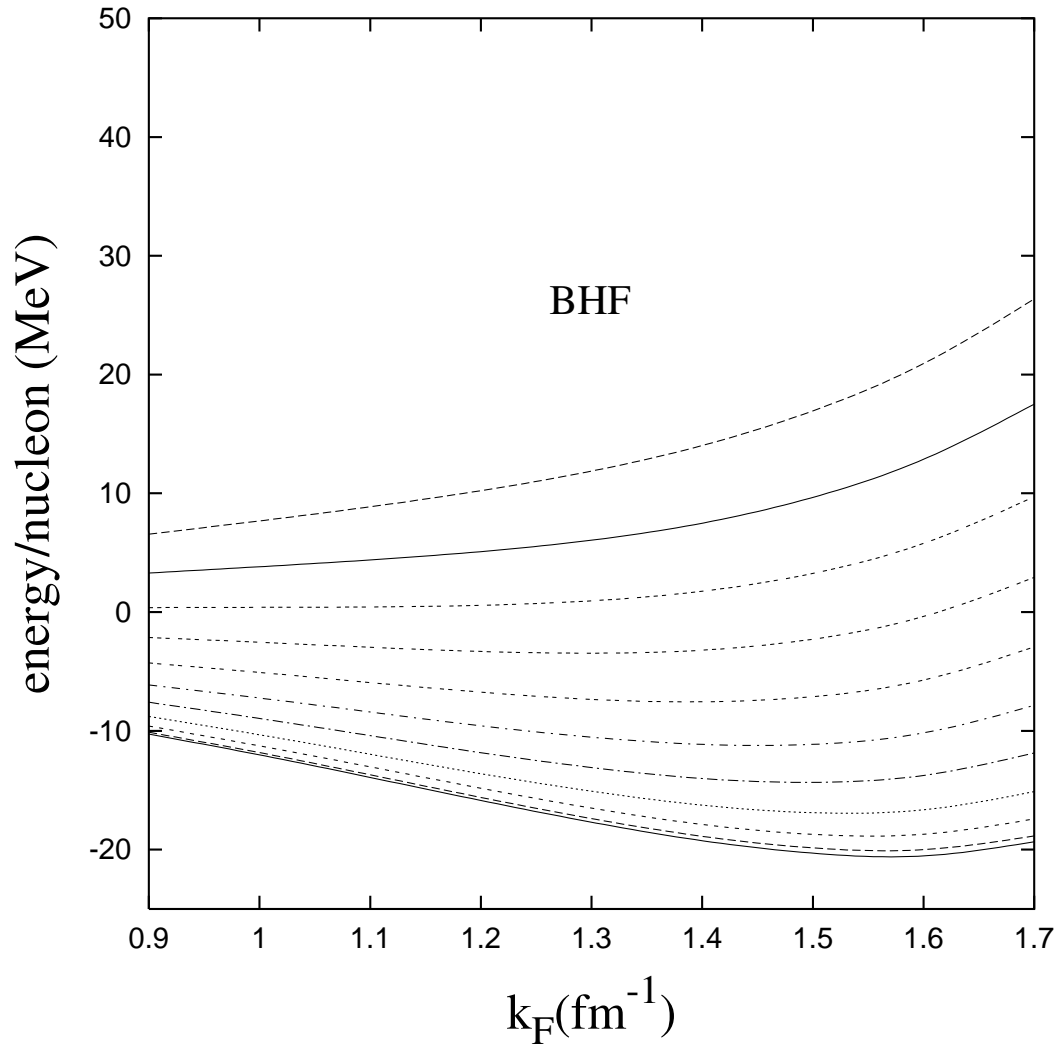


FIG. 4. Same as Fig. 3, but obtained from BHF calculation.

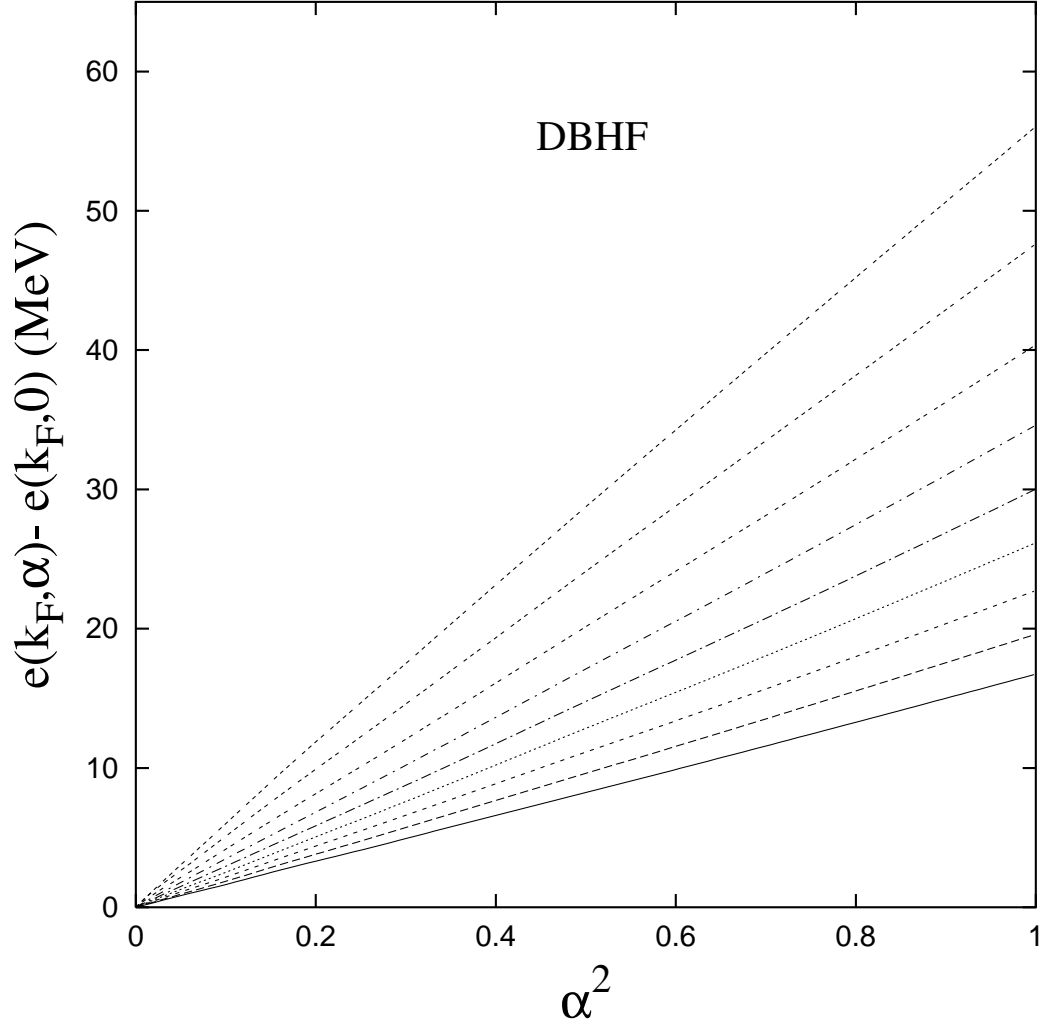


FIG. 5. The left-hand side of Eq. (20) versus α^2 (DBHF model) for increasing values of the Fermi momentum from 0.9 fm^{-1} (lowest curve) to 1.7 fm^{-1} .

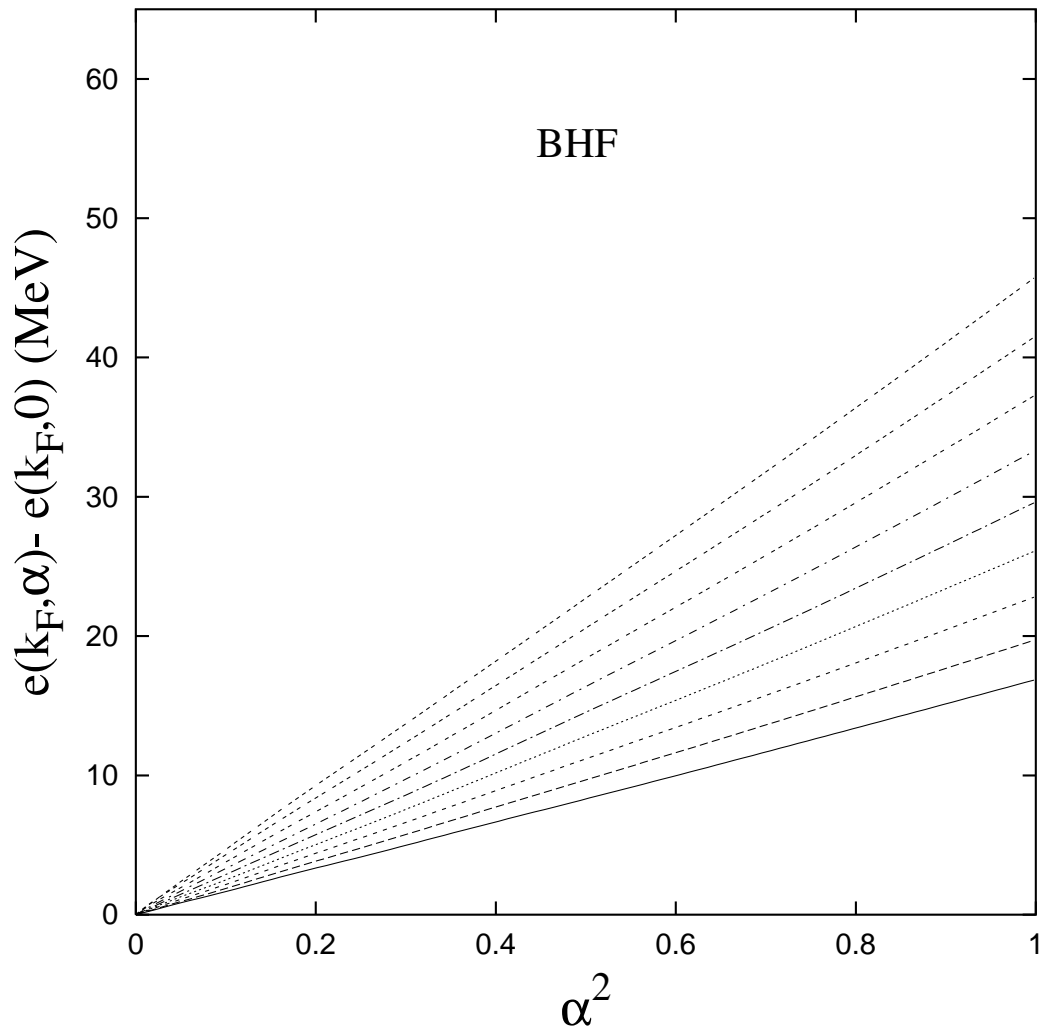


FIG. 6. As in Fig. 5, with the BHF model.

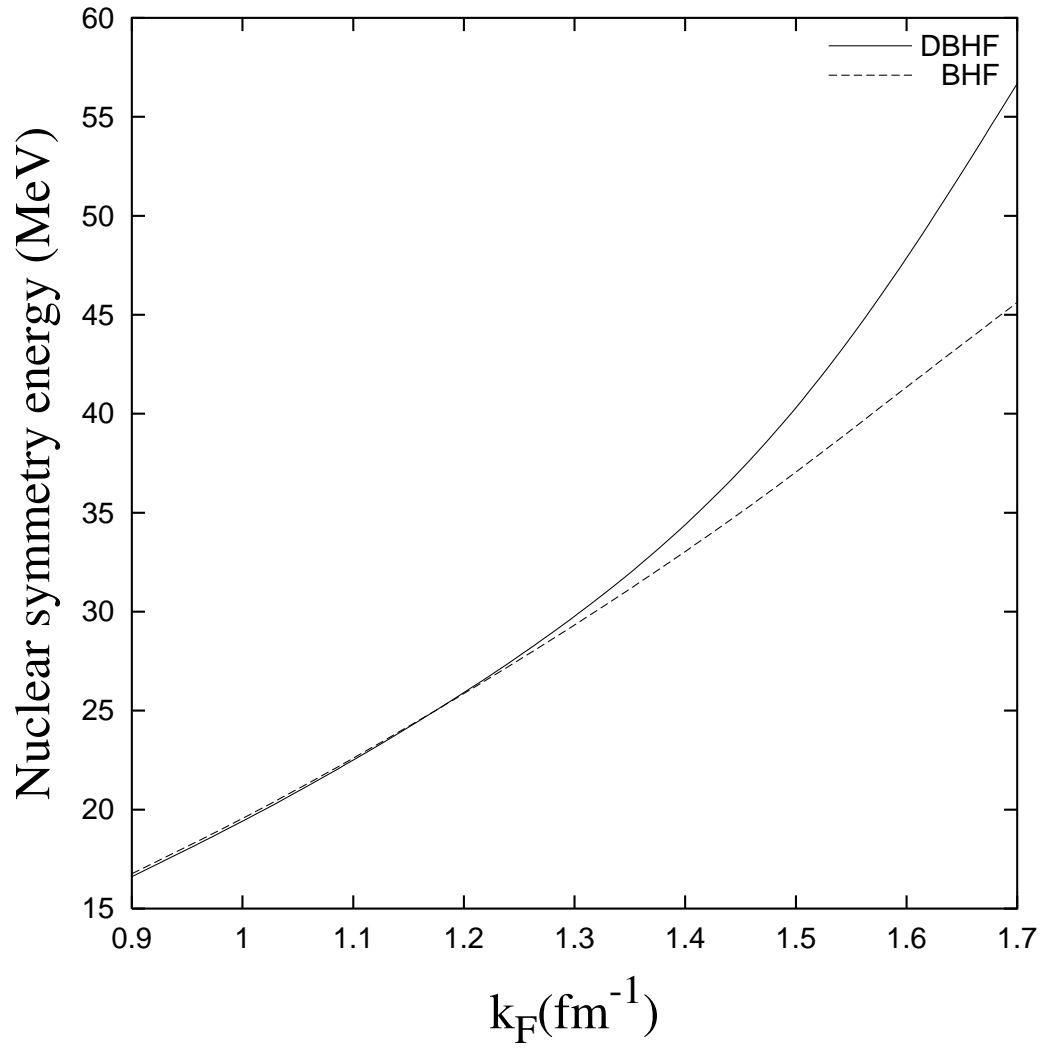


FIG. 7. Nuclear symmetry energy as a function of the Fermi momentum. The solid line is the prediction from DBHF calculation, while the dashed line is obtained with the conventional Brueckner approach.